Science in China Series D: Earth Sciences

www.scichina.com
earth.scichina.com
www.springerlink.com

Modeling gross primary production of a temperate grassland ecosystem in Inner Mongolia, China, using MODIS imagery and climate data

WU WeiXing[1,2], WANG ShaoQiang[1†], XIAO XiangMing[3], YU GuiRui[4], FU YuLing[4] & HAO YanBin[5]

[1] Qianyanzhou Ecological Experimental Station, Institute of Geographic Sciences and Natural Resources Research, Chinese Academy of Sciences, Beijing 100101, China;
[2] Graduate University of Chinese Academy of Sciences, Beijing 100049, China;
[3] Institute for the Study of Earth, Oceans and Space, University of New Hampshire, Durham, NH 03824, USA;
[4] Key Laboratory of Ecosystem Network Observation and Modeling, Institute of Geographic Sciences and Natural Resources Research, Chinese Academy of Sciences, Beijing 100101, China;
[5] Laboratory of Quantitative Vegetation Ecology, Institute of Botany, Chinese Academy of Sciences, Beijing 100093, China

Carbon fluxes in temperate grassland ecosystems are characterized by large inter-annual variations due to fluctuations in precipitation and land water availability. Since an eddy flux tower has been in operation in the Xilin Gol grassland, which belongs to typical temperate grassland in North China, in this study, observed eddy covariance flux data were used to critically evaluate the biophysical performance of different remote sensing vegetation indices in relation to carbon fluxes. Furthermore, vegetation photosynthesis model (VPM) was introduced to estimate gross primary production (*GPP*) of the grassland ecosystem for assessing its dependability. As defined by the input variables of VPM, Moderate Resolution Imaging Spectroradimeter (MODIS) and standard data product MOD09A1 were downloaded for calculating enhanced vegetation index (*EVI*) and land surface water index (*LSWI*). Measured air temperature (*Ta*) and photosynthetically active radiation (*PAR*) data were also included for model simulating. Field CO_2 flux data, during the period from May, 2003 to September, 2005, were used to estimate the "observed" *GPP* (GPP_{obs}) for validation. The seasonal dynamics of *GPP* predicted from VPM (GPP_{VPM}) was compared quite well (R^2=0.903, n=111, P<0.0001) with the observed *GPP*. The aggregate GPP_{VPM} for the study period was 641.5gC·m^{-2}, representing a ~6% over-estimation, compared with GPP_{obs}. Additionally, *GPP* predicted from other two typical production efficiency model (PEM) represents either higher overestimation or lower underestimation to GPP_{obs}. Results of this study demonstrate that VPM has potential for estimating site-level or regional grassland *GPP*, and might be an effective tool for scaling-up carbon fluxes.

GPP, eddy covariance, remote sensing, Xilin Gol

The eddy covariance technique has been widely used for continuous *in situ* observations of CO_2, H_2O and energy fluxes, and the resultant net ecosystem exchange (*NEE*) data have provided valuable information about gross primary production (*GPP*) and ecosystem respiration (*Re*) estimation[1]. Although the eddy covariance results are used to represent whole ecosystems, the sampling region is limited to a relatively small "footprint" (typically a few hectares or less)[2]. Additionally, the measurements are costly, time consuming, limited to relatively flat and uniform terrain, and cannot readily be

Received September 12, 2007; accepted July 1, 2008
doi: 10.1007/s11430-008-0113-5
†Corresponding author (email: sqwang@igsnrr.ac.cn)
Supported by International Partnership Project of Chinese Academy of Sciences (Grant No. CXTD-Z2005-1), National Basic Research Program of China (Grant No. 2002CB412501), and NASA Land Cover and Land Use Change (LCLUC) program (NAG5-11160, NNG05GH80G)

installed at many types of sites, leaving much of the world unsampled[3]. However, satellite remote sensing can provide synoptic coverage of large regions and systematic observation of ecosystems at regular time intervals. Therefore, remote sensing has played an increasing role in characterization of vegetation structure and estimation of primary production[4−8]. For integrating eddy covariance flux measurement and remote sensing, and for further studies of regional vegetation production and carbon cycle, *GPP* estimation could be used as an intermediate step[9].

Most satellite-based modeling studies have used production efficiency model (PEM) to estimate *GPP* at large spatial scales, e.g., TURC[5], MODIS-PSN[7], and GLO-PEM[8]. In these models, *GPP* is estimated as the product of $FPAR_{\text{canopy}}$, photosynthetically active radiation (*PAR*), and ε_g, where $FPAR_{\text{canopy}}$ is the fraction of *PAR* absorbed by vegetation canopy and ε_g is the light use efficiency (Table 1).

Table 1 Comparisons of different algorithms in the above-mentioned PEM[a)]

Model	$FPAR_{\text{canopy}}$	ε_g
TURC	$f(NDVI)$	ε_0
MODIS-PSN	$f(NDVI)$ $f(LAI)$	$\varepsilon_0 \times T \times VPD$
GLO-PEM	$f(NDVI)$	$\varepsilon_0 \times T \times SM \times VPD$

a) *NDVI*: normalized difference vegetation index; *LAI*: leaf area index; ε_0: maximum light use efficiency; *T*: air temperature scalar; *SM*: soil moisture scalar; *VPD*: water vapor pressure deficit scalar.

$FPAR_{\text{canopy}}$ is usually considered to be a function of *NDVI*, which is a greenness-related vegetation index, derived from reflectance in red and near-infrared wavebands[10]. However, many studies have found that *NDVI* can be affected by a number of different factors[11], some of which can potentially confound models of *GPP* simulation. Additionally, results of a study on comparing daily light use efficiency from four CO_2 flux tower sites (an agriculture field, a tallgrass prairie, a deciduous broadleaf forest, and a boreal forest) support inclusion of parameters for the phenological status of the vegetation in ε_g estimating[12].

Recently, a new satellite-based vegetation photosynthesis model (VPM) has been developed, and successfully applied to some different ecosystems for *GPP* modeling, based on conceptual partition of photosynthetically active vegetation (chlorophyll), non-photosynthetically active vegetation (NPV), innovative inclusion of improved vegetation indices and phenological status scalar[9,13−16]. The comparisons made by ecology station in the Harvard Forest have demonstrated that predicted *GPP* from VPM agreed well with observed *GPP* from flux tower (GPP_{VPM}=0.97 × GPP_{obs}, R^2=0.92, n=110, P<0.0001), while contemporary MODIS-PSN *GPP* products were clearly underestimated[13].

Since the VPM model has not been evaluated and applied in temperate grassland ecosystems[9,13−16], in this study, we chose the temperate semiarid steppe in Xilin Gol League as field study area. Our objectives of this research include: (1) to further examine biophysical performance of vegetation indices in relation to seasonal dynamics of CO_2 fluxes in temperature grassland ecosystem, and (2) to further evaluate the dependability of the VPM model for estimating *GPP* of the temperate grassland ecosystem.

1 Materials and methods

1.1 Study site

The selected temperate grassland is located in the center of Xilin Gol League, Inner Mongolia, China. Xilin Gol League covers a vast plain with an altitude more than 1000 m. The latitudinal and longitudinal ranges are 43°26′−44°39′N and 115°32′−117°12′E. For detailed description about the study site, refer to Table 2.

Table 2 Detailed information of geographic, climatic, and vegetation conditions about Xilin Gol temperate grassland site

Item	Description
Location	43°32′N, 116°40′E
Elevation (m)	1189
Annual mean air temperature (℃)	–0.4
Annual mean precipitation (mm)	350.9
Soil type	chestnut soil (3% organic matter)
Primary Vegetation	warm season grasses, such as Chinese Leymus (*Leymus chinensis*), Siberian Spearagrass (*Achnatherum sibiricum*)
Ecosystem type	semi-arid steppe
Observation period	2003-4-23－2005-9-22

1.2 Flux and climatic data

An eddy covariance flux tower (43°32′45″N, 116°40′30″E) has been operated nearly continuously at the grassland ecosystem site, measuring CO_2, H_2O, and energy fluxes since April 23, 2003 by the Chinese Terrestrial Ecosystem Flux Observational Network (ChinaFLUX), and is located near the Inner Mongolia Grassland Ecosystem Research Station of the Chinese Eco-

system Research Network (CERN)[17].

Original flux data were measured at the height of 2.2 m above the ground by an open-path eddy covariance system[18]. Details of quality assurance and quality control of the original data (e.g. coordinate rotation, WPL correction, invalid data filtering, friction velocity (u^*) correction) could be found in refs. [9, 18]. Annual complete gap-filled half-hourly *NEE* data with solar altitude less than 0 degree were used to estimate dark (nighttime) respiration. Relationship between nocturnal *NEE* and air temperature in the grassland ecosystem was determined by using Van't Hoff function, based on one year data[9]. The resultant regression equation was then used to predict ecosystem respiration during daytime (solar altitude greater than 0), combing with measured air temperature. *GPP* was finally estimated as *NEE* minus estimated daytime *Re*.

Additional meteorological factors (such as solar-radiation, net radiation and photosynthetic photon flux density, and relative humidity) have also been observed half-hourly. Some meteorological data were used for model simulation, including mean daily air temperature, and daily sum of *PAR*.

In order to run the VPM model, daily climate and CO_2 flux data were processed to the 8-day interval as defined by the 8-day composite MODIS images (Figure 1). We calculated the sums of *PAR* and CO_2 fluxes over 8-day periods, and the averages of daily air temperature over 8-day periods.

1.3 MODIS data and vegetation indices

Seven spectral bands of the 36 spectral bands in the MODIS sensor are primarily designed for the study of vegetation and other land surfaces: blue (459－479 nm), green (545－565 nm), red (620－670 nm), NIR (841－875 nm), NIR′ (1230－1250 nm), SWIR (1628-1652 nm), and SWIR′ (2105－2155nm). The MODIS sensor acquires daily images of the globe at a spatial resolution of 250 m for the red and NIR bands, and 500 m for the blue, green, NIR′, SWIR, and SWIR bands.

The MODIS Land Science Team provides a suite of standard data products for users, including the 8-day land surface reflectance product (MOD09A1) that has the seven spectral bands mentioned above at 500 m spatial resolution. The MODIS datasets are provided to users in a tile fashion; each tile covers approximately 10 latitudes by 10 longitudes (on an equal-area grid). We acquired the 8-day land surface reflectance product (MOD09A1) for the period from May, 2003 to September, 2005 from the Earth Observing System (EOS) Data Gateway (http://redhook.gsfc.nasa.gov/~imswww/pub/imswelcome/). Surface reflectance values from four spectral bands (blue, red, NIR and SWIR) were used to calculate three vegetation indices (*NDVI*, *EVI*, and *LSWI*). Based on the geographic information (latitude and longitude) of the CO_2 flux tower site at the grassland site of Inner Mongolia, data from the MOD09A1 product were extracted from one MODIS pixel (500

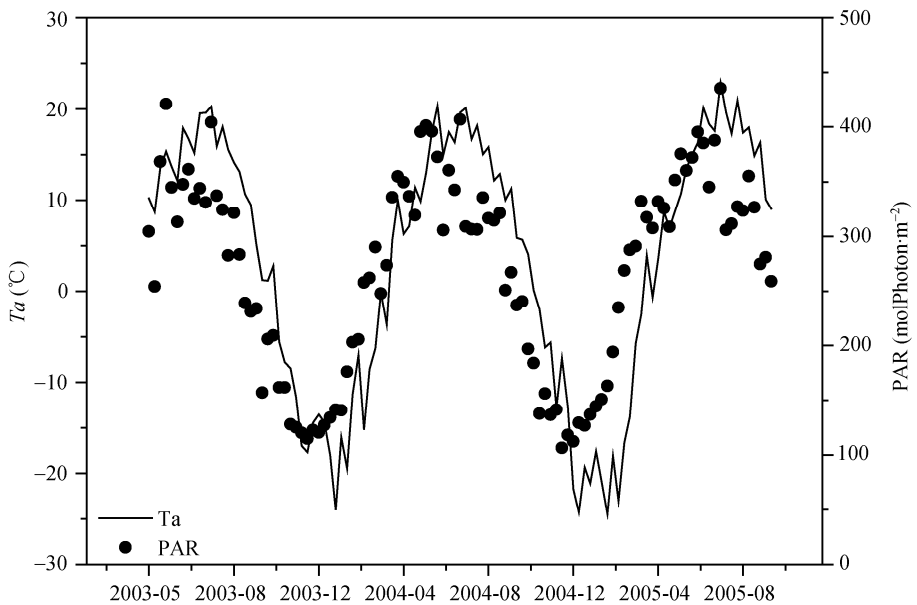

Figure 1 The seasonal dynamics of mean 8-day air temperature (*Ta*) and aggregate 8-day photosynthetically active radiation (*PAR*) from May 2003 to September 2005 at the grassland eddy flux tower site in Inner Mongolia, China.

m×500 m) centered on the flux tower[13−16]. An earlier study has already demonstrated that using one MODIS pixel had nearly the same reliability for analysis of vegetation indices and simulation of the VPM model as using 3×3 MODIS pixels and 5×5 MODIS pixels[15]. Simulations of the VPM model are driven by MODIS images in 2003—2005 temporally consistent with the available field data of 2003 to 2005.

We calculated *NDVI* and *EVI* using the equations below[10,11]:

$$NDVI = \frac{\rho_{\mathrm{NIR}} - \rho_{\mathrm{red}}}{\rho_{\mathrm{NIR}} + \rho_{\mathrm{red}}}, \quad (1)$$

$$EVI = 2.5 \times \frac{\rho_{\mathrm{NIR}} - \rho_{\mathrm{red}}}{\rho_{\mathrm{NIR}} + 1 + 6.0 \times \rho_{\mathrm{red}} + 7.5 \times \rho_{\mathrm{blue}}}, \quad (2)$$

where ρ is land surface reflectance of NIR, red or blue spectral band noted by subscripts. *EVI* includes the blue band for atmospheric correction[11]. The advanced optical sensors, such as MODIS and VEGETATION, have additional spectral bands (e.g., blue and shortwave infrared), making it possible to develop time-series data of improved vegetation indices[15]. *EVI* has recently been used for the study of temperate forests[15], and is much less sensitive to aerosols than *NDVI*[19].

Because the SWIR spectral band is sensitive to vegetation water content and soil moisture, a combination of NIR and SWIR bands has been used to derive water-sensitive vegetation indices, including the land surface water index (*LSWI*) (eq. (3))[13,20]:

$$LSWI = \frac{\rho_{\mathrm{NIR}} - \rho_{\mathrm{SWIR}}}{\rho_{\mathrm{NIR}} + \rho_{\mathrm{SWIR}}}. \quad (3)$$

As leaf water content or soil moisture increases, SWIR absorption increases and SWIR reflectance decreases, resulting in the increase of *LSWI* value. Recent work on evergreen needle-leaf forests has shown that *LSWI* is sensitive to changes in leaf water content over time[13].

2 Vegetation photosynthesis model

Leaves and plant canopies are composed of photosynthetically active vegetation (chlorophyll) and non-photosynthetic vegetation (NPV, e.g. stems, cell walls, and veins). Based on conceptual partitioning of chlorophyll and NPV, the VPM model was developed and successfully applied to estimating *GPP* of forests[13−16] and alpine[9] ecosystems.

2.1 Model description

A brief description of the VPM model was given below:

$$GPP = \varepsilon_{\mathrm{g}} \times FPAR_{\mathrm{chl}} \times PAR, \quad (4)$$

$$\varepsilon_{\mathrm{g}} = \varepsilon_0 \times T_{\mathrm{scalar}} \times W_{\mathrm{scalar}} \times P_{\mathrm{scalar}}, \quad (5)$$

where *PAR* is the photosynthetically active radiation ($\mu\mathrm{molPhoton} \cdot \mathrm{m}^{-2} \cdot \mathrm{s}^{-1}$), $FPAR_{\mathrm{chl}}$ is the fraction of *PAR* absorbed by chlorophyll, and ε_{g} is the light use efficiency ($\mu\mathrm{molCO_2} \cdot \mu\mathrm{molPhoton}^{-1}$). The parameter ε_0 is the apparent quantum yield or maximum light use efficiency ($\mu\mathrm{molCO_2} \cdot \mu\mathrm{molPhoton}^{-1}$), and T_{scalar}, W_{scalar} and P_{scalar} are three down-regulation scalars for the effects of temperature, water, and leaf phenology on the light use efficiency of vegetation, respectively.

In the current version of the VPM model, $FPAR_{\mathrm{chl}}$ is assumed to be a linear function of *EVI*, and the coefficient *a* in eq. (6) is simply set to be 1.0[13−16]:

$$FPAR_{\mathrm{chl}} = a \times EVI. \quad (6)$$

T_{scalar} is estimated using the equation developed for the terrestrial ecosystem model[21]:

$$T_{\mathrm{scalar}} = \frac{(T - T_{\min})(T - T_{\max})}{(T - T_{\min})(T - T_{\max}) - (T - T_{\mathrm{opt}})^2}, \quad (7)$$

where $T_{\min}$, $T_{\max}$ and T_{opt} are minimum, maximum, and optimal temperatures for photosynthetic activities, respectively. When air temperature falls below $T_{\min}$, T_{scalar} is set to 0.

W_{scalar}, the effect of water on plant photosynthesis, has been estimated as a function of soil moisture and/or vapor pressure deficit (*VPD*) in other production efficiency models[7−8]. As a first order of approximation, we proposed an alternative and simple approach that uses a satellite-derived water index to estimate the seasonal dynamics of W_{scalar}[13]:

$$W_{\mathrm{scalar}} = \frac{1 + LSWI}{1 + LSWI_{\max}}, \quad (8)$$

where $LSWI_{\max}$ is the maximum *LSWI* within the plant-growing season for an individual pixel.

P_{scalar} is included to account for the effect of leaf phenology (leaf age) on photosynthesis. The calculation of P_{scalar} is dependent upon the longevity of leaves (deciduous, versus evergreen). For a canopy dominated by leaves with a life expectancy of 1 year (one growing season, e.g., deciduous trees), P_{scalar} is calculated at two different phases as a linear function[14]. Because grass-

land canopies have new leaves emerging throughout much of the plant growing season, P_{scalar} is set to be 1.0[9] in this study.

2.2 Parameterization for VPM

The VPM model has three sets of parameters: maximum light use efficiency (ε_0); maximum *LSWI* of the plant growing season ($LSWI_{max}$); three temperature parameters for photosynthetic activities (T_{min}, T_{max}, and T_{opt}).

The values of ε_0 vary with vegetation types, and information about ε_0 for individual vegetation types can be obtained from a survey of the literature and/or analysis of nearly instantaneous *NEE* of CO_2 and photosynthetic photon flux density (*PPFD*) at a CO_2 eddy flux tower site based on a linear or a nonlinear regression[13,22].

In the study of the VPM model, ε_0 values were derived from the hyperbolic function (Michaelis-Menten equation) using eight-day half-hourly daytime *NEE* and *PPFD* data during the plant growing season (May to September). Therefore, we calculate ε_0 from each eight-day periodic data of this grassland ecosystem based on Michaelis-Menten equation, and then choose the best fit of a year for deriving the annual value of ε_0 (Table 3). The resultant maximum light efficiency is 0.0167, 0.0248, and 0.0054 μmol $CO_2 \cdot$ μmolPhoton^{-1} for 2003, 2004, and 2005, respectively. We found mid-day (noon) photosynthetic declines in diurnal curve because of light saturation for all the eight-day periods in 2005[18]. Therefore, we only used half-hourly daytime *NEE* and *PPFD* data when *PPFD* was lower than 1200 μmolPhoton $\cdot$ m$^{-2} \cdot$ s^{-1} to estimate ε_0 in 2005 (Figure 2).

Table 3 Parameters of Michaelis-Menten equation for fitting *NEE* and *PPFD* data

	2003	2004	2005
Day of year	162－169	210－217	226－233
Maximum light use efficiency (μmol$CO_2 \cdot$ μmolPhoton^{-1})	0.0167	0.0248	0.0054
Maximum light-saturation photosynthesis rate (mg$CO_2 \cdot$ m$^{-2} \cdot$ s^{-1})	0.210	0.374	0.167
R^2	0.549	0.669	0.150
n	240	230	169

The second parameter set is for calculation of W_{scalar}. The maximum *LSWI* value within the plant-growing season was selected as an estimate of $LSWI_{max}$. As a parameter describing water state, $LSWI_{max}$ varies with years with different environmental conditions. We chose the maximum *LSWI* values during the plant growing

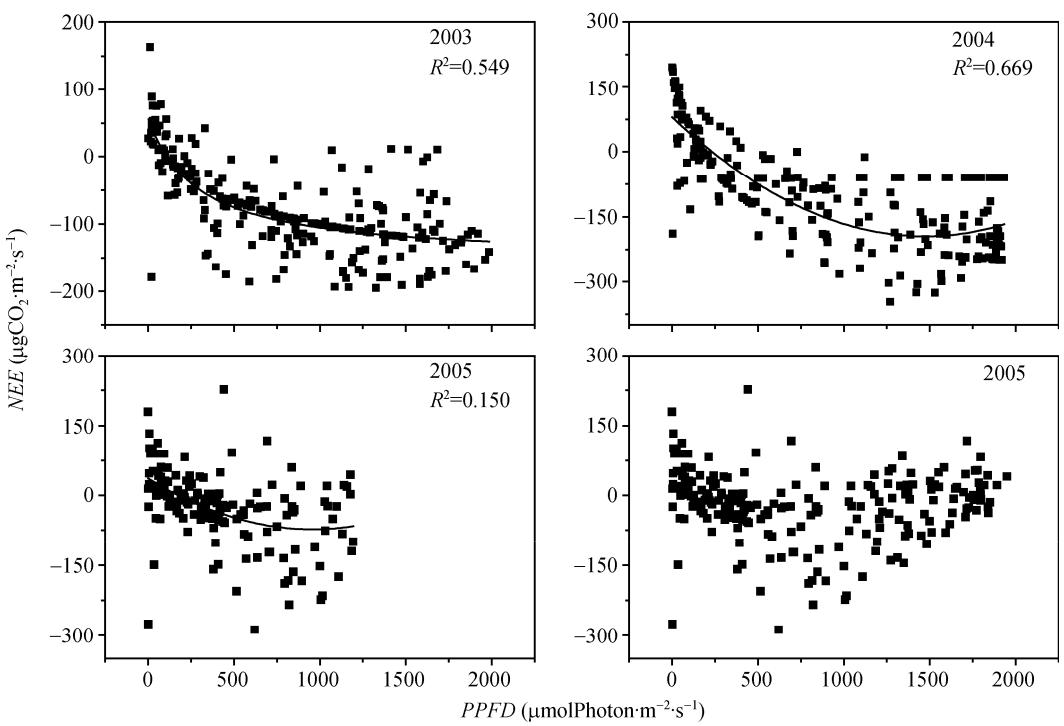

Figure 2 The half-hourly daytime *NEE* and *PPFD* data in eight-day period of the growing seasons (2003-06-11－2003-06-18; 2004-07-28－2004-08-04; 2005-08-14－2005-08-21) which fits best the hyperbolic function in each year. The left-below panel illustrates all the half-hourly daytime *NEE* and *PPFD*

data from August 14, 2005 to August 21, 2005. There is a clear decline of absolute values of *NEE* date when *PPFD* is larger than 1200 μmolPhoton·m^{-2}·s^{-1}.

season in a year as $LSWI_{max}$. $LSWI_{max}$ values are 0.076 (July 12, 2003) for 2003, 0.019 (July 19, 2004) for 2004, and −0.058 (August 13, 2005) for 2005, respectively (Figure 3).

The third parameter set is used for calculation of T_{scalar}. We analyzed the relationship between daily air temperature data and daily observed *GPP* data in 2004 at the grassland eddy flux tower site because there were the most optimal climatic conditions in 2004 for the three investigating years. We estimated a minimum temperature (T_{min}) of 6℃, optimum temperature (T_{opt}) of 17 ℃, and maximum temperature (T_{max}) of 21 ℃ throughout the whole study period for this grassland ecosystem[9] (Figure 4).

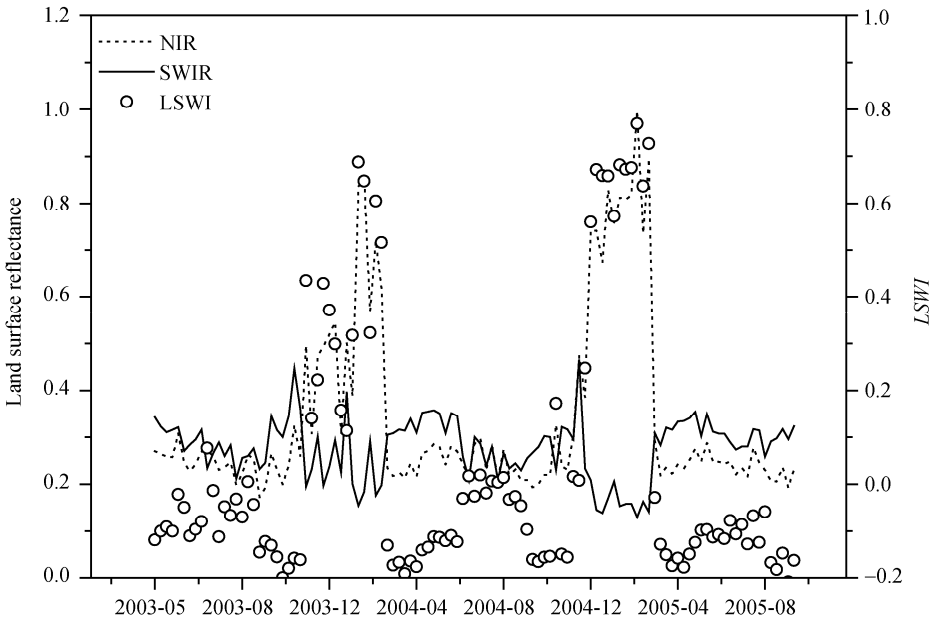

Figure 3 The seasonal dynamics of land surface water index (*LSWI*) and land surface reflectance of near infrared (NIR) and short wave infrared (SWIR) wavebands, which are extracted and calculated from MOD09A1 from May 2003 to September 2005 at the grassland eddy flux tower site. We chose the maximum growing season *LSWI* in each year to be used as $LSWI_{max}$ for yearly *GPP* simulation.

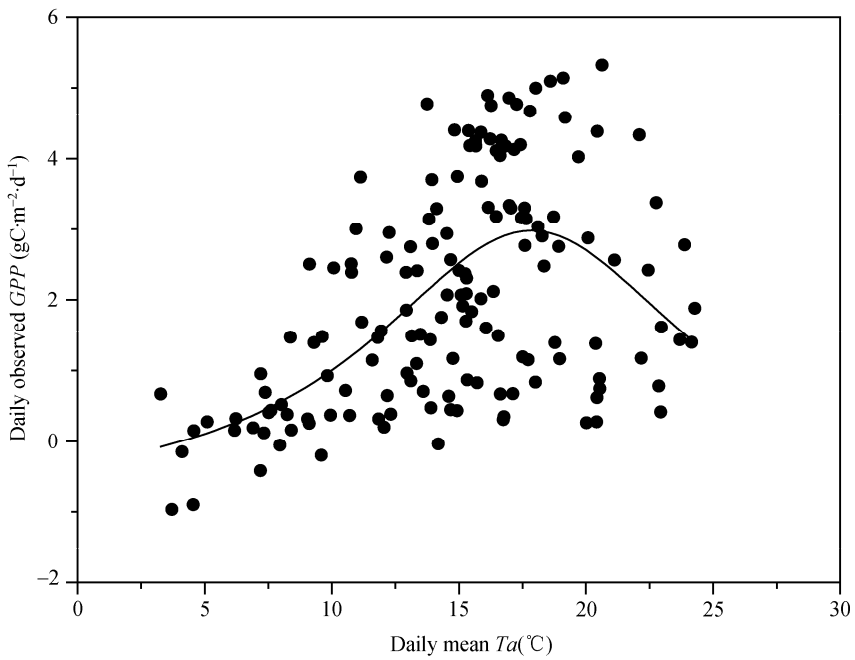

Figure 4 The relationship between mean daily air temperature data and sum of daily observed *GPP* (GPP_{obs}) during the growing season of the year 2004, clearly showing that *GPP* starts to decrease when air temperature gets to over 17℃.

3 Results

3.1 Seasonal dynamics of *NDVI* and *EVI* from eight-day MODIS images

Seasonal dynamics of land surface reflectance values, which were extracted from the standard eight-day MODIS land surface reflectance products (MOD09A1), show distinct seasonal variations of red, NIR, and blue bands. During the plant growing season (from May to October), the values of near infrared (NIR) band (841—875 nm) are greater than those of red (620—670 nm) and blue bands (459—479 nm) (Figure 5).

Seasonal dynamics of *EVI* within the plant growing season at this grassland site differs substantially from that of *NDVI*. The maximum *EVI* values in summer were 0.36 in 2003, 0.35 in 2004, and 0.31 in 2005, which are much lower than the maximum *NDVI* values (0.62 in 2003, 0.61 in 2003, and 0.57 in 2003) (Figure 6).

The seasonal dynamics and their differences in *NDVI* and *EVI* signals suggest that we could assume *FPAR* estimated using a function of *NDVI* is likely to represent the *FPAR* absorbed by all "green" vegetation, but *FPAR* estimated using a function of *EVI* might represent the *FPAR* absorbed by leaf chlorophyll. Apart from the plant growing seasons, the values of *EVI* and *NDVI* are very low (approximately 0), indicating that these two vegetation indices could well be used to delineate growing season transitions (at the time when *GPP* declines rapidly). Within growing seasons, dynamics of *EVI* matches GPP_{obs} somewhat better than those of *NDVI* (Figure 7).

3.2 Seasonal dynamics of *LSWI* from eight-day MODIS images

Under a semi-arid temperate climate, grassland vegetation canopies are generally sparse. This mixture of green plants and soils might be sensed by satellite sensors from space. As shown in Figure 3, *LSWI* values during the plant growing season (May to October) are generally low, sometimes even below zero. Cumulative rainfall during the plant growing season was 122.1 mm in 2003, 335.9mm in 2004, and 133.7mm in 2005, respectively. *LSWI* values in 2004 were a little larger than those in 2003 and 2005 (Figure 3), therefore, it is suggested that inter-annual changes of *LSWI* values during the plant growing season could reflect the rainfall differences between wet year (2004) and dry years (2003, 2005). In addition, the values of *LSWI* in the seasons except the plant growing season are much higher (Figure 3), similar to the earlier studies on the forest and alpine ecosystems[13,15]. Extremely high *LSWI* values in winter and early spring are attributed to snow cover. Snow cover

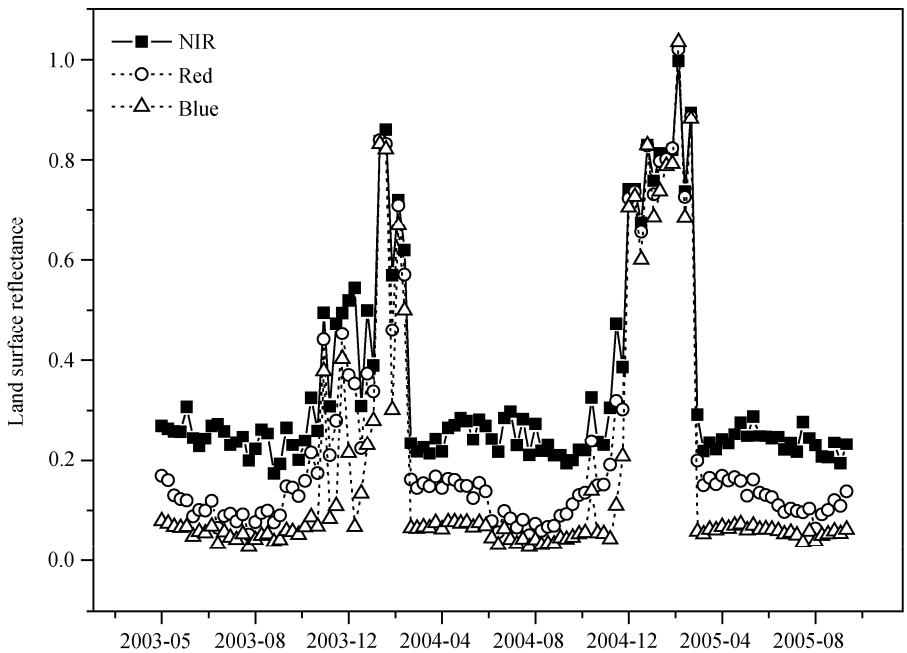

Figure 5 The seasonal dynamics of land surface reflectance of individual spectral band (NIR, red, and blue) from May 2003 to September 2005 at the grassland eddy flux tower site in Inner Mongolia, China. Note that in plant growing seasons (annually, May to September), land surface reflectance of near infrared (NIR) is clearly higher than reflectances of blue and red wavebands. In the seasons except the plant growing seasons, they are close to each other

with irregular fluctuations, but have little influence on the model simulation because the air temperature then is below the minimum photosynthetic temperature (T_{min}).

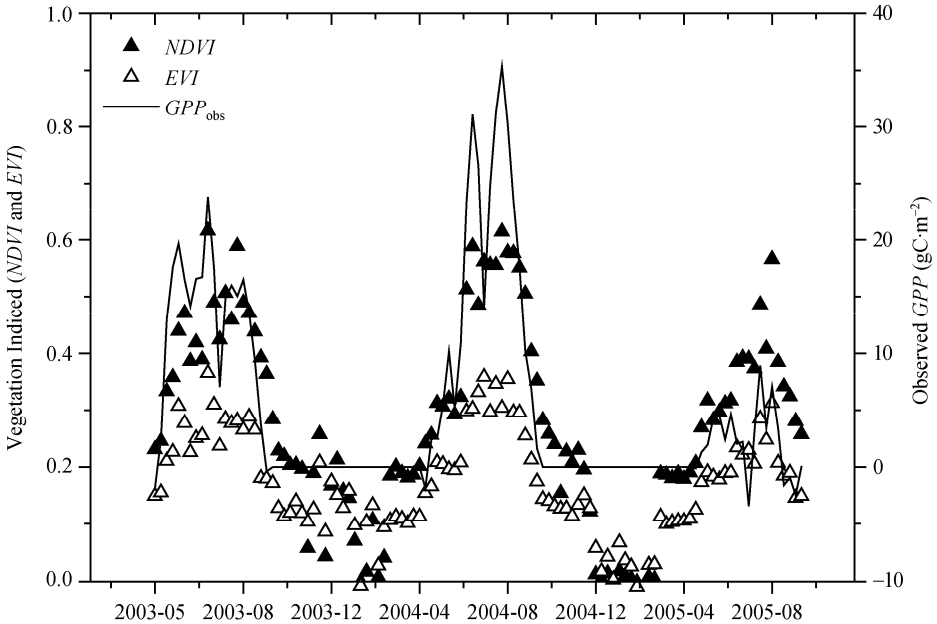

Figure 6 The seasonal dynamics of normalized difference vegetation index (*NDVI*) and enhanced vegetation index (*EVI*) and observed *GPP* data (GPP_{obs}) from May 2003 to September 2005 at the grassland eddy flux tower site in Inner Mongolia, China. All the *NDVI* data are higher than *EVI* data in growing seasons. The seasonal dynamics of GPP_{obs} is somewhat different from that of *NDVI* and *EVI* partly due to the calculation procedure of GPP_{obs}, especially in 2005.

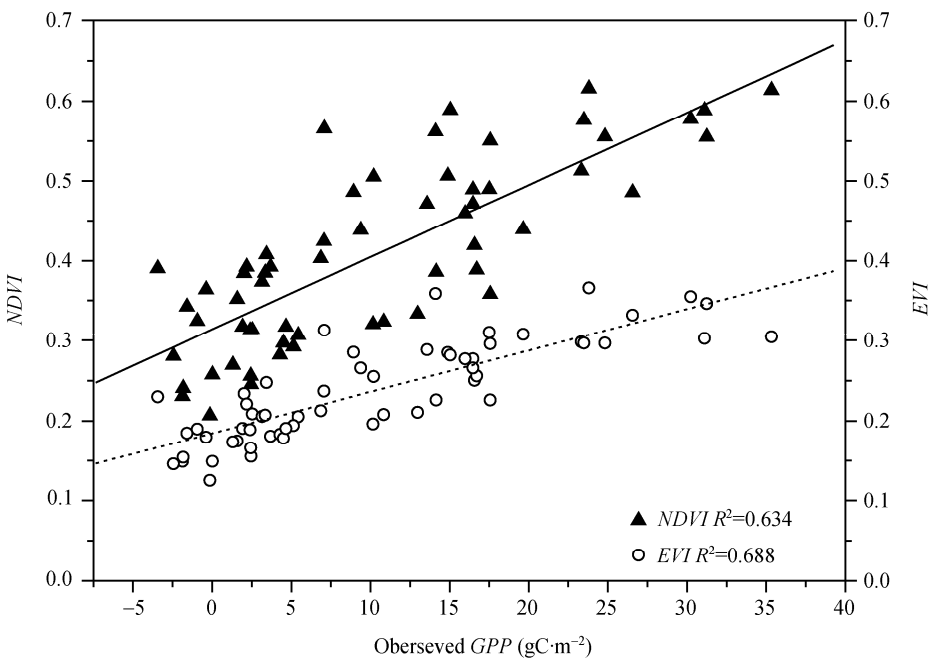

Figure 7 The relationships between vegetation indices (*NDVI*, *EVI*) and observed *GPP* data calculated from observed field *NEE* data, demonstrating that *EVI* matches *GPP* slightly better than *NDVI* at the grassland eddy flux tower site.

has very high reflectance values in visible and NIR spectral bands but relatively low reflectance values in shortwave infrared[20]. During the winter and early spring, the land surface is a mixture of vegetation and snow, which likely results in anomalously high *LSWI* values. As spring progresses, air temperature increases, the snow cover gradually melts, resulting in a decline of *LSWI* values.

The seasonal dynamics of land surface reflectance (near infrared and short wave infrared spectral bands) is also illustrated in Figure 3. Note that the values of the short wave infrared spectral band are a little higher than those of near infrared spectral band during the plant growing season. However, as time progresses, the differences become smaller, resulting in an *LSWI* increasing, which can be seen in the same figure.

3.3 Simulation of the VPM model via eight-day MODIS imagery and climate data

The parameters T_{scalar}, W_{scalar}, and P_{scalar} are three down-regulation scalars for *GPP* simulation. T_{scalar} is strongly affected by the maximum, minimum, and optimal temperature parameters. In the dormant seasons, air temperatures were all below minimum photosynthetic temperature, so the T_{scalar} values then were set to be 0. In the plant growing seasons, the values of T_{scalar} experienced large fluctuations related to air temperature, especially in 2005. Irregular fluctuations during the plant growing seasons (May and July) could also be found. This behavior due to air temperature then was close to maximum temperature for photosynthesis. The scalar for describing water effect on vegetation photosynthesis in this study (W_{scalar}) was calculated from *LSWI* using eq. (8). This parameter also experiences some large fluctuations in the dormant season, but because T_{scalar} was set to be 0 due to the lower air temperature (Figure 8), the large changes in *LSWI* during the non-plant growing seasons were not important for *GPP* modeling. While calculating P_{scalar}, as mentioned above, we set all the P_{scalar} values to unity for grassland ecosystems.

Using the calculated scalars, estimated parameters and measured climate data, we simulated *GPP* for the Inner Mongolia grassland site using the VPM model. The seasonal dynamics agrees well with the dynamics of *GPP* derived from *in situ* flux data from May, 2003 to September, 2005 (Figure 9). The VPM model tracked the major features of the observed *GPP* data during the study period closely, although the magnitudes were not entirely consistent.

The GPP_{VPM} values from 2004 matched with observed *GPP* a little better than those in 2003 and 2005, which were both drought years with less effective precipitation. However, primary production of temperate grasslands in China is highly sensitive to inter-annual variation in climate, especially to the change in precipitation[23,24]. Therefore, gross primary productivity in 2003 and 2005 was smaller (Figure 9).

Furthermore, the simple linear comparison between simulated *GPP* and observed *GPP* also shows a good relationship, although the values of simulated *GPP* were somewhat larger than those of observed *GPP* (Figure 9). Calculated total *GPP* during the study time was 641.5 $\text{gC}\cdot\text{m}^{-2}$ and 603.8 $\text{gC}\cdot\text{m}^{-2}$ for modeling *GPP* and observation *GPP*, respectively. The modeled *GPP* overestimates the observed *GPP* by about 6%.

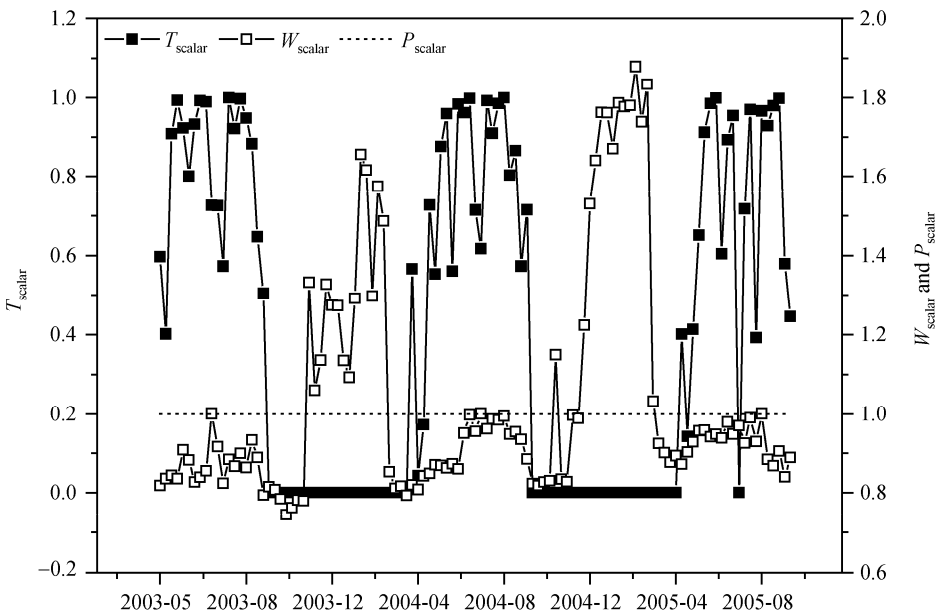

Figure 8 Seasonal dynamics of temperature, water and phenology down-regulation scalars. Note that T_{scalar} shows clear undulations in the plant growing seasons, while W_{scalar} is relatively flat with small changes. In addition, P_{scalar} was set to 1 during the investigating period.

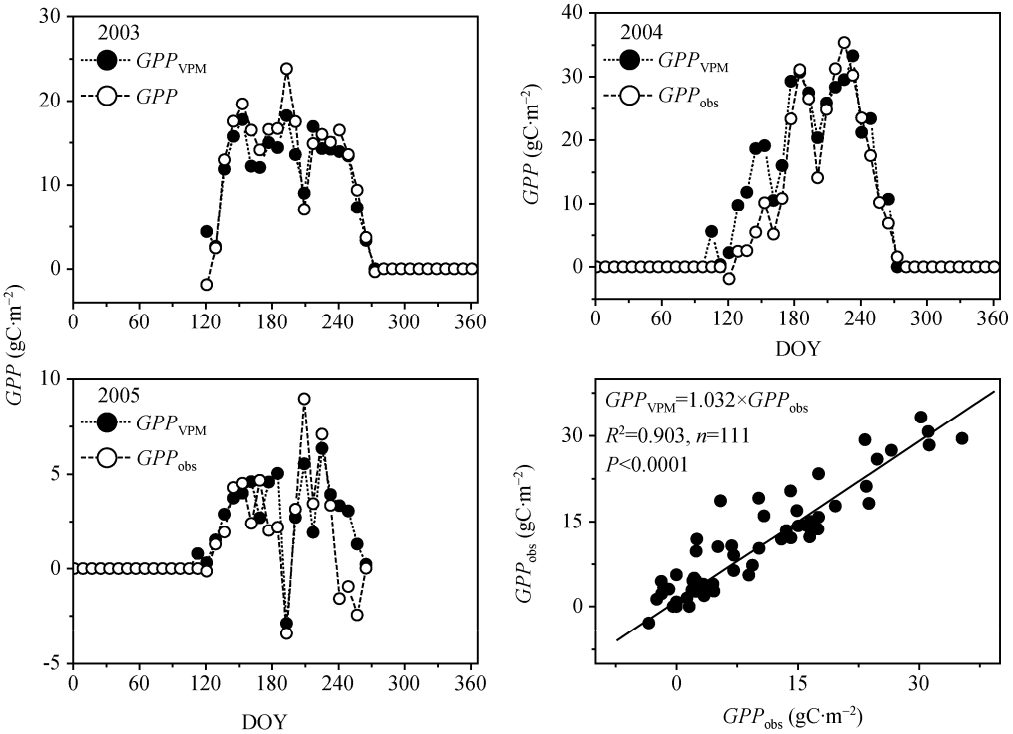

Figure 9 The seasonal dynamics of GPP_{VPM} (simulation of the VPM model) and GPP_{obs} (*GPP* calculated from the filed *NEE* data) at the grassland eddy flux tower site (DOY means day of year). The right-below panel illustrates a linear relationship between simulated *GPP* (GPP_{VPM}) and calculated *GPP* (GPP_{obs}) over the period of May 2003 to September 2005.

4 Discussion and summary

We note two particularly interesting results from this study, which correspond with earlier studies of the VPM model[9,13−16]. The first is that *EVI* still has a slightly stronger linear relationship with observed *GPP* than *NDVI* does in this grassland ecosystem. One of the advantages of the VPM model is to use *EVI* instead of *NDVI* to represent the "greenness" of vegetation. In the earlier studies, *EVI* had quite better linear relationship with *GPP*. For example, for the Harvard Forest (deciduous forest), the correlation coefficient of *NDVI* and *GPP* was 0.64, while that of *EVI* and *GPP* was 0.84[14], and this is largely attributed to saturation of *NDVI* with high values of leaf area index in the forest. In comparison, grassland vegetation in semi-arid regions generally has low values of leaf area index, and saturation of *NDVI* is not an issue. In this study, we still found that the correlation coefficient of *EVI* and *GPP* was slightly greater than that of *NDVI* and *GPP* (Figure 7). In addition, we also found that the *NDVI* values in Figure 7 were more widely scattered than *EVI* values. This result supports the notion that using *EVI* for *GPP* simulation in the VPM model is an improvement relative to other PEM using *NDVI* (Table 1). Secondly, the VPM model uses a novel remote-sensing index related to vegetation water content (e.g., *LSWI* in this study) to estimate the effect of water availability on canopy photosynthesis. One advantage of using a water-related vegetation index in the VPM model is that there is no need for a soil moisture model. In this study, we found remote sensing water-related scalar (W_{scalar}) could reflect the rainfall differences between wet year (2004) and dry years (2003, 2005) (Figure 8). We argue that these models are usually driven by very coarsely resolved input datasets (e.g., precipitation, soil texture, and soil depth), which results in large uncertainty in soil moisture.

The multi-year simulations of the VPM model have shown that in general, there is a good agreement between GPP_{VPM} and GPP_{obs} from 2003 to 2005. However, there still exist large differences between GPP_{obs} and GPP_{VPM} in a few 8-day periods, for instance, larger GPP_{VPM} from May to July of 2004 (Figure 10). Those discrepancies might be due to the following reasons.

First, we found that selection of photosynthesis parameters T_{min}, T_{max} and T_{opt} is likely to have some impacts on T_{scalar}, and therefore will affect *GPP* estimation. The values we used for the above three temperature parameters differ from other studies[9,13−16] (Figure 4). Second, the error in observed *GPP* is also an another important factor[25,26]. For a given amount of *NEE* measured by the eddy-covariance method, an error in estimation of daily respiration would result in an equivalent error in estimation of *GPP*. The two major steps that must be taken to derive *GPP* are the gap filling of *NEE* and estimation of daytime *Re*. Both the two steps require subjective decisions, including empirical model selection, and are currently the subject of a lot of discussion[26].

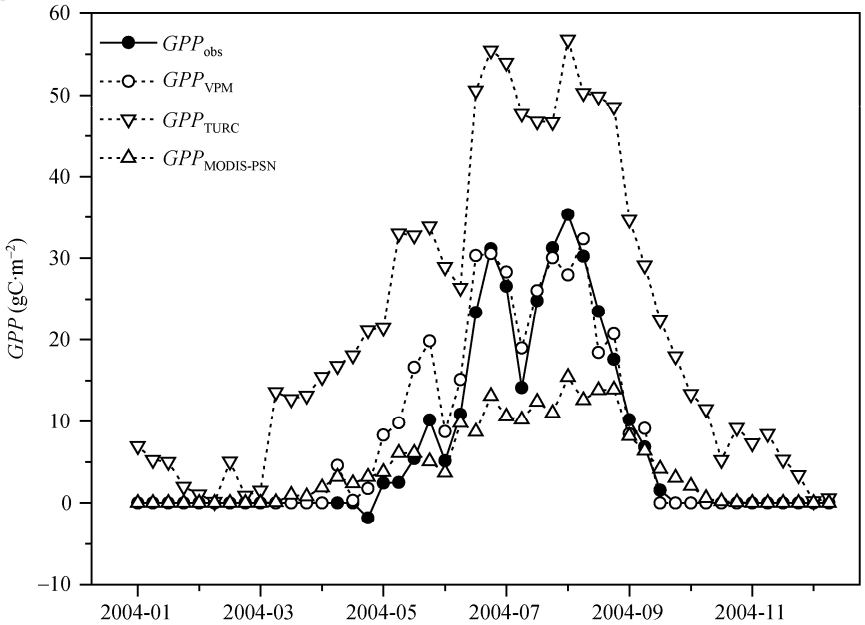

Figure 10 The seasonal dynamics of predicted *GPP* from different PEM and observed *GPP* from flux tower in 2004. Subscript labels TURC and MODIS-PSN mean different PEM mentioned above. Filled Circle represent the observed *GPP* form eddy covariance *NEE* data; open symbols represent predicted *GPP* from different PEM. *GPP* from TURC was clearly overestimated during the whole year, while *GPP* from MODIS-PSN was underestimated during the growing season. VPM did not work well during the early period of the growing season, however, the seasonal dynamics match well with that of the observed *GPP*.

However, compared with other PEM (such as TURC and MODIS-PSN), VPM works much better. In Figure 10, we use observed PAR and remote sensing *NDVI* to calculate GPP_{TURC} following ref, [5], and downloaded *GPP* products (MOD17A2) from EOS Data Gateway (http://redhook.gsfc.nasa.gov/~imswww/pub/imswelcome/) to get $GPP_{MODIS-PSN}$ (1×1 pixel) during the best environmental year, 2004. Clearly, during the whole year, *GPP* from TURC was overestimated because it set maximum light use efficiency as actual light use efficiency[5]. *GPP* from MODIS-PSN was underestimated during the growing season for the grassland site, which might be due to over-correction of *VPD* on light use efficiency in 2004[8].

Furthermore, we used remotely sensed spectral bands to characterize water effects on vegetation photosynthesis. Although *LSWI* distinctly revealed the water stress in 2003 and 2005 at this grassland site (Figure 3), we are still not sure whether it could exactly track the changes of vegetation water content. That to what degree canopy water content can be retrieved from satellite images is an important research issue for remote sensing science[27−29].

In summary, simulation of the VPM model in this semi-arid temperate grassland ecosystem provides relatively accurate estimates of *GPP* in all wet and dry years. The eddy covariance measurements have shown that grasslands at the site had distinct seasonal dynamics and moderate inter-annual variation in *GPP* from 2003 to 2005, which may be due to climatic variations (e.g. extreme drought) during the research period. The VPM model is capable of tracking seasonal dynamics and inter-annual variations in *GPP* of this temperate semi-arid steppe at a sub-monthly (8-day in this study) temporal resolution. As more modeling studies would be carried

out in the future, long-term objective of VPM is to use the model to simulate global gross primary production or net primary production at finer temporal and spatial resolutions.

The authors thank Dr. Bobby Braswell for his comments and suggestions, and two anonymous reviewers for their critical and advisable comments on the earlier version of the manuscript. Thanks also go to Zhang Mi for data analyzing; *Zhou Lei for manuscript revising.*

1 Falge E, Baldocchi D, Tenhunen J, et al. Seasonality of ecosystem respiration and gross primary production as derived from FLUXNET measurements. Agric For Meteorol, 2002, 113: 53－74
2 Moncreiff J B, Malhi Y, Leuning R. The propagation of errors in long-term measurements of land-atmosphere fluxes of carbon and water. Glob Change Biol, 1996, 2: 231－240
3 Running S W, Baldocchi D D, Turner D P, et al. A global terrestrial monitoring network integrating tower fluxes, flask sampling, ecosystem modeling, and EOS satellite data. Remote Sens Environ, 1999, 70: 108－127
4 Liu J, Chen J M, Cihlar J, et al. Net primary productivity mapped for Canada at 1-km resolution. Glob Ecol Biogeogr, 2002, 11: 115－129
5 Ruimy A, Dedieu G, Saugier B. TURC: A diagnostic model of continental gross primary productivity and net primary productivity. Glob Biogeochem Cycle, 1996, 10: 269－285
6 Field C B, Randerson J T, Malmström. Global net primary production: Combing ecology and remote sensing. Remote Sens Environ, 1995, 51: 74－88
7 Heinsch F A, Reeves M, Votava P, et al. User's Guide: GPP and NPP (MOD17A2/A3) Products NASA MODIS Land Algorithm, Version 2.0, 2003
8 Goetz S J, Prince S D, Goward S N, et al. Satellite remote sensing of primary production: An improved production efficiency modeling approach. Ecol Model, 1999, 122: 239－255
9 Li Z Q, Yu G R, Xiao X M, et al. Modeling gross primary production of alpine ecosystems in the Tibetan Plateau using MODIS images and climate data. Remote Sens Environ, 2007, 107: 510－519
10 Tucker C J. Red and photographic infrared linear combinations for monitoring vegetation. Remote Sens Environ, 1979, 8: 127－150
11 Huete A, Didan K, Miura T, et al. Overview of the radiometric and biophysical performance of the MODIS vegetation indices. Remote Sens Environ, 2002, 83: 195－213
12 Turner D P, Urbanski S, Bremer D, et al. A cross-biome comparison of daily light use efficiency for gross primary production. Glob Change Biol, 2003, 9: 383－395
13 Xiao X M, Hollinger D, Aber J D, et al. Satellite-based modeling of gross primary production in an evergreen needle leaf forest. Remote Sens Environ, 2004, 89: 519－534
14 Xiao X M, Zhang Q Y, Braswell B, et al. Modeling gross primary production of temperate deciduous broadleaf forest using satellite images and climate data. Remote Sens Environ, 2004, 91: 256－270
15 Xiao X M, Zhang Q Y, Hollinger D, et al. Modeling gross primary production of an evergreen needleleaf forest using MODIS and climate data. Ecol Appl, 2005, 15: 954－969
16 Xiao X M, Zhang Q Y, Saleska S, et al. Satellite-based modeling of gross primary production in a seasonally moist tropical evergreen forest. Remote Sens Environ, 2005, 94: 105－122
17 Yu G R, Wen X F, Sun X M, et al. Overview of ChinaFLUX and evaluation of its eddy covariance measurement. Agric For Meteorol, 2006, 137: 125－137
18 Fu Y L, Yu G R, Sun X M, et al. Depression of net ecosystem CO_2 exchange in semi-arid Leymus chinensis steppe and alpine shrub. Agric For Meteorol, 2006, 137: 234－244
19 Xiao X M, Braswell B, Zhang Q, et al. Sensitivity of vegetation indices to atmospheric aerosols: Continental-scale observations in Northern Asia. Remote Sens Environ, 2003, 84, 385－392
20 Xiao X M, Boles S, Liu J Y,et al. Characterization of forest types in northeastern China, using multitemporal SPOT-4 VEGETATION sensor data. Remote Sens Environ, 2002, 82: 335－348
21 Raich J W, Rastetter E B, Melillo J M, et al. Potential net primary productivity in South-America —— application of a global-model. Ecol Appl, 1991, 1: 399－429
22 Gilmanov T G, Verma S B, Sims P L, et al. Gross primary production and light response parameters of four southern plains ecosystems estimated using long-term CO_2-flux tower measurements. Glob Biogeochem Cycle, 2003, 1071, doi: 10.1029/2002GB002023
23 Xiao X M, Ojima D S, Parton W J, et al. Sensitivity of Inner Mongolia grasslands to climate change. J Biogeogr, 1995, 22: 643－648
24 Chen Z Z, Wang S P. Typical Steppe Ecosystems of China (in Chinese). Beijing: Science Press, 2000. 104－120
25 Richardson A D, Braswell B H, Hollinger D Y, et al. Comparing simple respiration models for eddy flux and dynamic chamber data. Agric For Meteorol, 2006, doi: 10.1016/j.agrformet.2006.10.010
26 Falge E, Baldocchi D, Olson R, et al. Gap filling strategies for long term energy flux data sets. Agric For Meteorol, 2001, 107: 71－77
27 Penuelas J, Pinol J, Ogaya R, et al. Estimation of plant water concentration by the reflectance water index WI (R900/R970). Int J Remote Sens, 1997, 18: 2869－2875
28 Sims D A, Gamon J A. Estimation of vegetation water content and photosynthetic tissue area from spectral reflectance: A comparison of indices based on liquid water and chlorophyll absorption features. Remote Sens Environ, 2003, 84: 526－537
29 Champagne C M, Staenz K, Bannari A, et al. Validation of a hyperspectral curve-fitting model for estimation of plant water content of agricultural canopies. Remote Sens Environ, 2003, 87: 148－160